Icarus 220 (2012) 305–310

Contents lists available at SciVerse ScienceDirect

Icarus

journal homepage: www.elsevier.com/locate/icarus

Upper limits on the size of satellites of Asteroid (4) Vesta from 2007 Hubble Space Telescope observations

Lucy A. McFadden [a,*], Fabienne A. Bastien [a,1], Max Mutchler [b], Carolyn A. Crow [a,2], Heather Weir [a,c], Jian-Yang Li [a], Douglas P. Hamilton [a]

[a] Department of Astronomy, University of Maryland, College Park, MD 20742, USA
[b] Space Telescope Science Institute, 3700 San Martin Drive, Baltimore, MD 21218-2463, USA
[c] Science Systems Applications, 10210 Greenbelt Rd., Suite 600, Lanham, MD 20706, USA

ARTICLE INFO

Article history:
Received 1 July 2011
Revised 2 May 2012
Accepted 2 May 2012
Available online 17 May 2012

Keywords:
Asteroid Vesta
Satellites of asteroids
Hubble Space Telescope observations

ABSTRACT

We imaged the region around Asteroid (4) Vesta in nine long exposures using the Wide Field Planetary Camera 2 on the Hubble Space Telescope on May 14 and 16, 2007 to conduct a deep search for satellites in support of NASA's Dawn mission that orbited (4) Vesta in 2011–2012. Several previous search efforts have been undertaken, but no satellites were detected. Our search covered distances from 14 to 260 Vesta radii and searched to a limiting magnitude of 22.5 ± 0.4 in HST's wide-band red filter (F702W). Our upper limit for possible satellites corresponds to a satellite just 22 ± 4 m in radius, assuming the same optical properties as Vesta. Our upper limit is ~10 times smaller than the best limit of previous searches. *In situ* satellite searches by NASA's Dawn spacecraft will probe regions closer to Vesta than our effort reported here.

Published by Elsevier Inc.

1. Introduction

Asteroid (4) Vesta is the third largest main belt asteroid in our Solar System with a mean radius of 265 ± 5 km (Thomas et al., 1997a,b). It also is one of the brightest main belt asteroids with a high visible geometric albedo, p_H, of 0.37, determined from magnitude measurements calibrated to its light curve, phase function and a radius derived from a stellar occultation (Li et al., 2011; Shevchenko and Tedesco, 2006; Tedesco et al., 2002). Vesta's reflectance spectrum has the same major absorption bands as the basaltic achondrite meteorites known as howardites, eucrites, diogenites (HEDs) (e.g. McCord et al., 1970; Feierberg and Drake, 1980), making it compositionally different from other large main belt asteroids. In addition, it has long been known that some smaller asteroids, called vestoids, have similar spectral features and therefore compositional similarities to Vesta (Binzel and Xu, 1993), suggesting that they may be remnants of one or more collisions between Vesta and other bodies (e.g. Asphaug, 1997). This theory is supported by disk resolved Hubble Space Telescope images taken in 1996 showing a large crater-like feature in Vesta's southern hemisphere suggestive of an impact basin 230 km in radius, almost as large as the asteroid's radius. Its existence suggests that a nearly catastrophic collision occurred between Vesta and another primordial asteroid (Thomas et al., 1997a).

In this paper we present the results of a satellite search conducted around Asteroid (4) Vesta with Hubble Space Telescope in 2007. Our search has two primary motivations. First, the theory that large collisions like the one responsible for the suspected southern hemisphere impact basin may produce satellites (Durda et al., 2004). Secondly, NASA's Dawn spacecraft mission to two large asteroids, (1) Ceres and (4) Vesta is in orbit around (4) Vesta at the time of this writing. The presence of natural satellites could have serious implications for mission operations and navigation.

Previous efforts to search for satellites of (4) Vesta yielded no satellites to varying limits of detection (Fig. 1). Gehrels et al. (1987) conducted a search between 46 and 1894 Vesta radii (12,190 and 501,900 km) using direct CCD imaging and found nothing greater than 1–2 km in radius. Gradie and Flynn (1988) searched between 21 and 400 Vesta radii (5565 and 106,000 km) using coronagraphic imaging and found nothing 180 m or larger in radius. Roberts et al. (1995) searched from 1.13 to 17.2 Vesta radii from its surface (300 to 4445 km) using speckle interferometry and found nothing larger than 51 ± 2 km radius. In our study, we searched the region around Vesta from ~14 to 260 Vesta radii (3710 to 68,900 km) and report here an upper limit of 22 ± 4 m radius. The outer edge of our search region is just beyond one half of Vesta's Hill radius of ~500 Vesta radii. No known satellites orbit

* Corresponding author. Present address: NASA Goddard Space Flight Center, Mail Code 160, Greenbelt, MD 20771, USA. Fax: +1 301 286 1655.
E-mail address: lucy.mcfadden@nasa.gov (L.A. McFadden).
[1] Present address: Vanderbilt University, 6301 Stevenson Center, Nashville, TN 37235, USA.
[2] Present address: Department of Earth and Space Sciences, University of California, Box 951567, Los Angeles, CA 90095, USA.

0019-1035/$ - see front matter Published by Elsevier Inc.
http://dx.doi.org/10.1016/j.icarus.2012.05.002

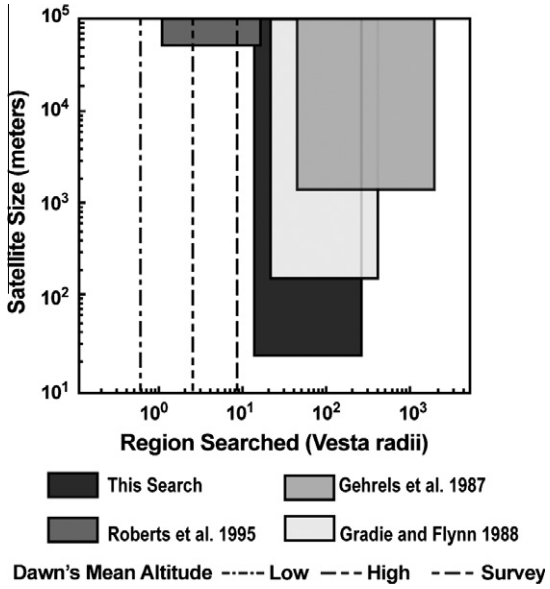

Fig. 1. This figure illustrates the size and region of space covered in this study (black) and in previous satellite searches of Vesta (lighter shades). The distance from Vesta is in units of Vesta's mean radius (265 km). The orbital altitudes of NASA's Dawn spacecraft are denoted as vertical hatch marks representing low, high and survey altitude mean orbits. The Dawn spacecraft will be in regions that have not been searched for satellites.

at such great distances and the region is not dynamically stable over long timescales (Hamilton and Burns, 1991).

2. Observations

The Hubble Space Telescope's Wide Field Planetary Camera 2 (WFPC2) observed Vesta on May 14 and May 16, 2007, to both search for satellites and map its surface (Li et al., 2010a). We used the F702W filter, a wide band red filter centered at 694 nm with $\Delta\lambda$ = 148 nm (McMaster et al., 2008) for this search and collected three sets of 40-s exposures. The first set consists of five successive images taken on May 14th, and the two subsequent sets of two images each obtained on May 16th. The data from May 14th allow for the most thorough search because the five consecutive images could be median filtered to remove cosmic rays, greatly reducing the possibility of confusing image artifacts and cosmic rays with possible satellites. Vesta's angular diameter was 0.620 arcsec at the time of our observations. Observing circumstances are listed in Table 1.

WFPC2 consists of 4 separate cameras: 3 Wide Field cameras (WFs) and 1 Planetary Camera (PC). Fig. 2a shows a single 40 s exposure including all four cameras. The WF cameras have a combined field of view of 2.5 × 2.5′ (Fig. 3) and a pixel scale of 0.1″/pixel. This corresponds to 84 km/pixel at Vesta's distance from Earth during the May 14th observations. The PC has a field of view of 35 × 35″ (Fig. 3) and a pixel scale of 0.046″/pixel (McMaster et al., 2008), corresponding to 39 km/pixel at the time when Vesta was observed. All the images are saturated in the vicinity of Vesta to a distance of ~14 Vesta radii due to the intentionally long exposures designed to search for small, faint satellites.

Table 1
Observing circumstances.

UTC date and time	r (AU)	Δ (AU)	α (°)	Filename
14 May 2007 19:06:16–19:12:16	2.15	1.18	9.5	u9q6040cm-gm
16 May 2007 20:40:16–20:42:16	2.15	1.17	8.5	u9q6050fm-gm
16 May 2007 23:54:16–23:56:16	2.15	1.17	8.5	u9q6070em-fm

r = heliocentric distance, Δ = geocentric distance, α = phase angle, filename = root-name of file in Hubble Space Telescope archive.

3. Search approach

3.1. Image processing

We applied standard pipeline corrections to these data, including bias and dark subtractions and a flat field correction. We summed five consecutive images from May 14, 2007, tracking Vesta and readily showing background stars as repeated parallel trails due to the telescope's tracking on Vesta (Fig. 2b). Simple summed images (where cosmic rays have not been rejected) and an exposure weight-map file recording artifacts and rejected pixels help distinguish CCD artifacts and residual cosmic rays from candidate satellites. To prepare the frames for blink-comparison searching, we combined individual mosaic (including all 4-chips), distortion-corrected images and cleaned them of most cosmic rays and star trails with a median filter using the IRAF/PyRAF/STSDAS tasks named, drizzle and imcombine (Fig. 2c). We also applied unsharp-masking, a digital enhancement process in which a Gaussian model of the original is subtracted from the original image. We apply this to the clean, combined images in order to create an image with a flatter dynamic range making it easier to identify faint candidate satellites (Fig. 2d). We performed the same image processing to the May 16th images. But, with only two consecutive images, we were unable to apply median filtering and the reduced images consequently have more artifacts. For this reason, we concentrated on the May 14th data, and used the May 16th observations primarily for follow-up.

3.2. Examining images

We individually read, aligned and displayed as frames in SAOImage DS9, v.5.3 (Joye and Mandel, 2003) the series of images from the three data sets, including the single raw frames, the exposure weight map, and the summed, median filtered, and unsharp-masked images. Next we systematically scanned the unsharp-masked image by eye for signals above the background, and marked the locations where the signal appeared as a point-spread function. We investigated each location in the other images to see if the signal qualified as a possible satellite detection. Positive detection criteria required the signal (1) exist in each individual raw and processed frame, (2) not have a low weight factor for any of the pixel locations, (3) not be a combination of a star and a cosmic ray, which when overlapping appear to be a trail with different motion than the background stars, and (4) not be any other image artifact referenced in chapter 4 of McMaster et al. (2008). We conducted a second search where we aligned the raw images by the World Coordinate System in SAOImage and blinked between the frames. The background stars remain fixed by this procedure while any satellite and Vesta would move relative to the registered background stars.

4. Results

We found no objects satisfying our detection criteria for satellites of Vesta. We did find and identify stars, artifacts, and an Asteroid 2004 PN34 (at RA 16:47:41 and Dec −13:50:46 on May 14, 2007 with an apparent magnitude of 19.8 and moving at −8.25 ± 0.13 km/s relative to Earth). The May 16th images produced more possible candidates, but we were unable to identify all sources because there were not enough images to remove cosmic rays. The remaining analysis in this paper involves determining the magnitude limits of our search first by establishing the

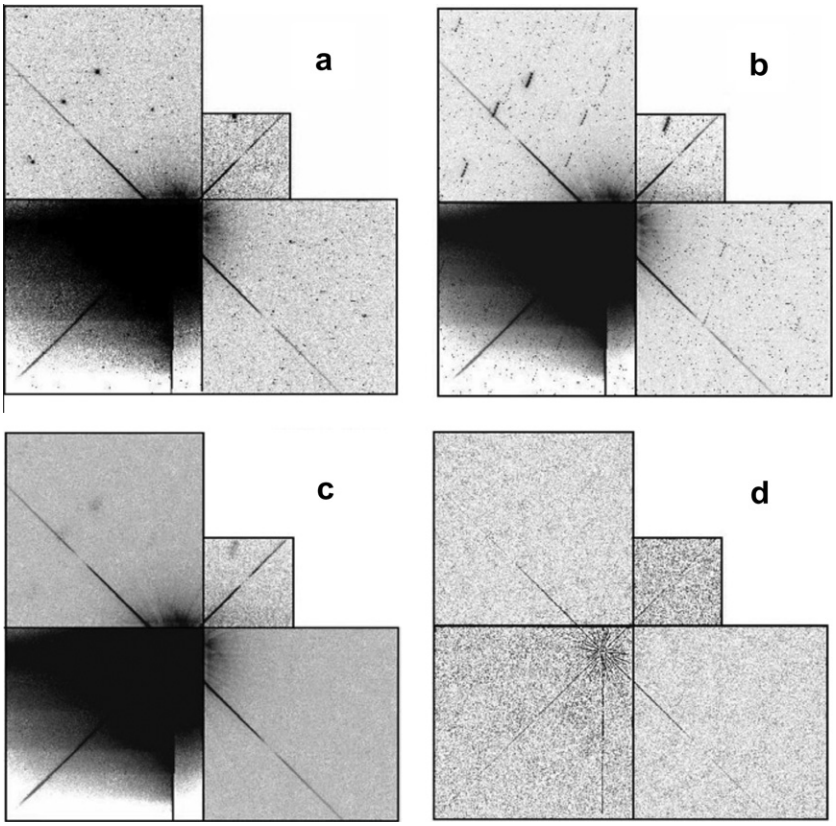

Fig. 2. Each panel shows one step of the image processing. (a) A single 40 s calibrated image including all four camera frames. (b) The sum of all images from one data set. Star trails are visible due to HST's tracking of Vesta. (c) Combined, median filtered image with most cosmic rays removed. (d) Unsharp-masked image used to look for satellites. The images are from the May 14, 2007 observations.

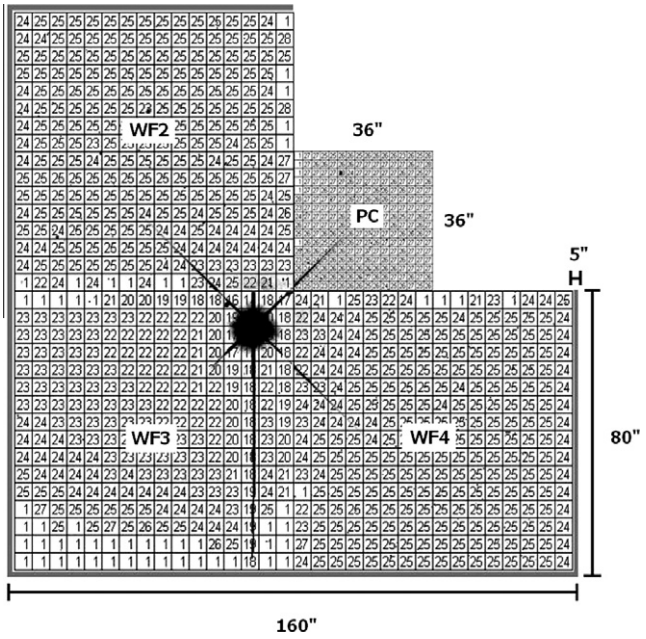

Fig. 3. A map of background magnitude as a function of position on the WFPC2 cameras, named Wide Field (WF) 2, 3 and 4 and Planetary Camera (PC). Camera dimensions are in arcsec. Regions labeled "1" denote areas where the average pixel value is negative because the detector is saturated and no meaningful magnitude could be calculated. The saturation near Vesta that leads to bleeding of the signal extends to both edges of the chip.

magnitude of the sky background and then including the instrument function and human factors.

5. Upper limits of detection

We first determined the sky background magnitudes, establishing the fact that the detection limits will vary primarily due to differing amounts of scattered Vesta light on the different cameras. We then took into account the telescope's point-spread function and devised an approach accounting for human factors that also contributes to satellite detection limits. We created synthetic satellite candidates with Gaussian point spread functions of different magnitudes and randomly implanted them into the images. Twenty-eight volunteers then searched to identify them. This approach is similar in concept to that of Steffl et al. (2006). Both sky background calculation and observer-limited detections with the telescope system's point spread function are described below.

5.1. Sky background

We define the background magnitude as the average magnitude of the sky background within a given area. This magnitude is calculated by

$$m = -2.5\log[\mathrm{DN}/\mathrm{exptime} * \mathrm{PHOTFLAM}] + \mathrm{PHOTZPT} - 5\log(r) - 5\log(\Delta) \quad (1)$$

where PHOTFLAM is the inverse sensitivity and has a value of 1.872439E−18 ergs cm^{-2} Å^{-1} DN^{-1}, and PHOTZPT is the HST magnitude zero point has a value of −21.1 magnitudes (Gonzaga et al., 2010). Both are HST photometry keywords from the image headers (McMaster et al., 2008), and PHOTZPT is defined such that the calculated source magnitude corresponds to a visual magnitude on the standard Johnson photometric system (e.g. Cox, 2000). DN is the data number, or measured flux in a pixel, exptime is the exposure

time (40 s) for each image, r is heliocentric distance of Vesta in astronomical units (AU), and Δ is Vesta's geocentric distance (AU) at the time of observations.

To determine the background magnitude we divided each image of 800 × 800 pixels into 50 × 50 pixel-bins for a total of 256 bins for each image. We calculated the average pixel value of each bin and inserted this DN value into Eq. (1) to obtain the magnitude of the background in that region. Fig. 3 is the background map as a function of position. In general, the background magnitude is 22 close to Vesta, and 25 further out. The planetary camera (PC) is however, more sensitive, and the background magnitude can be as faint as 28 magnitude. This sky background map serves to illustrate the uneven detection limits of our search.

5.2. Observer-limited detection

Realistically, we would expect actual detection limits to be worse than the background magnitudes calculated above due to the nature of the instrument's point spread function that is spread out over multiple pixels. The introduction of human error also affects detection limits. We therefore developed a test to estimate true visual detection limits taking into account factors for detecting an object that stays in a single pixel during the exposure. We wrote an IDL procedure that randomly implants satellites with two-dimensional Gaussian profiles into the raw images with random coordinates and magnitudes, ranging from magnitude 19 to 24. We restricted this analysis to the May 14th dataset of five successive images, analyzing each camera separately. Satellites were added to the images that were then median filtered. The IDL procedure also produced a separate output file containing the satellites' coordinates and magnitudes. Our test procedure to determine background limit assumes that a potential satellite has an orbital velocity that does not take it from one pixel to another between exposures. This is a reasonable assumption as circular orbital velocities at 14 and 260 Vesta radii are 68 and 16 m/s, respectively, and the pixel scale is 84 km and 39 km/pixel for WF and PC cameras, respectively. Any potential satellite would remain in one pixel over the time interval of observations on May 14th. The test results in an observer limit of detection.

We selected one of the brighter field stars in the images to be our standard star on which we scaled the magnitudes of implanted satellites. Using the US Naval Observatory B1.0 catalog to obtain its observed magnitude, we measured its flux. This value and the definition of the magnitude difference

$$M_1 - M_2 = 2.5 \log\left(\frac{F_2}{F_1}\right) \quad (2)$$

allow us to control the amplitude of an implanted satellite representing its magnitude. "M_1" and "M_2" are the magnitudes of the objects of interest, and "F_1" and "F_2" are their corresponding measured fluxes.

We selected 28 volunteers to search for our artificial satellites who had a range of experience from novice to expert. Seven of our data images were implanted with synthetic satellites that include the camera and telescope's point spread function. Twenty-eight individuals who were initially unfamiliar with the data were asked to view groups of 3–4 images using SAOImage DS9 display software (Joye and Mandel, 2003) and to identify possible satellites. The first image that each tester viewed contained synthetic satellites that were brighter than the expected visual magnitude limit in order to allow testers to become familiar with the software and process of discovering a satellite. After each tester completed the search, we manually determined and recorded which implanted satellites had been detected. Fig. 4 illustrates a DS9 displayed image with implanted satellites with circles noting the ones that were detected.

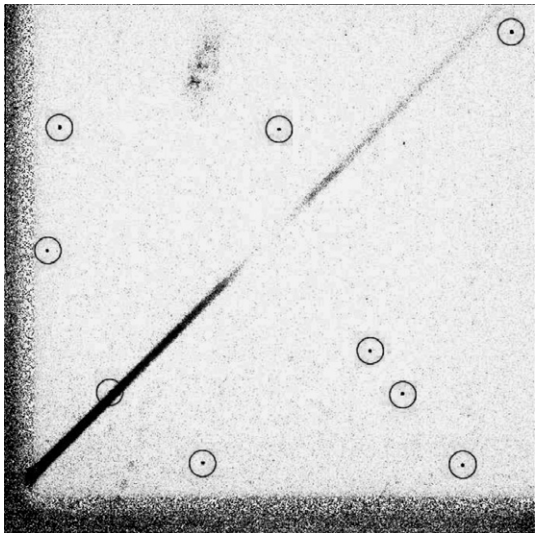

Fig. 4. DS9 displayed PC camera image with randomly implanted, synthetic satellites identified by the open circles. The synthetic satellites covered a range of magnitudes from above our estimated detections limit (as in this image) to well below the background noise. The satellite that falls on the diffraction spike serves to illustrate that the positions of satellites, which were randomly generated, simulate a multitude of possible observing circumstances and that an experienced observer could identify an object in this situation.

We find that the detection capability of WF2, WF4, and PC are similar in that the testers found all magnitude 22 "satellites" in these cameras. The limiting magnitudes, defined as the value for which satellites were detected with 50% efficiency, are 22.8 ± 0.2, 23.0 ± 0.2, and 23.0 ± 0.2 respectively, with PC being more sensitive due to its smaller pixel size. WF3's limiting magnitude of 22.3 ± 0.2 is lower than the others because Vesta was placed on this camera and its saturation and resulting scattered light controlled both the distance from Vesta that could be searched and the limiting magnitude of detection. In Fig. 5 we combined the results of the test described above for all four cameras in order to define a single value representing an upper limit. Examination of the plot shows that satellites to magnitude 22.3 were detected with 80–100% efficiency meaning that 80–100% of the implanted satellites of that magnitude were found. The detection efficiency drops at magnitudes fainter than 22. Correct identifications in all cameras were

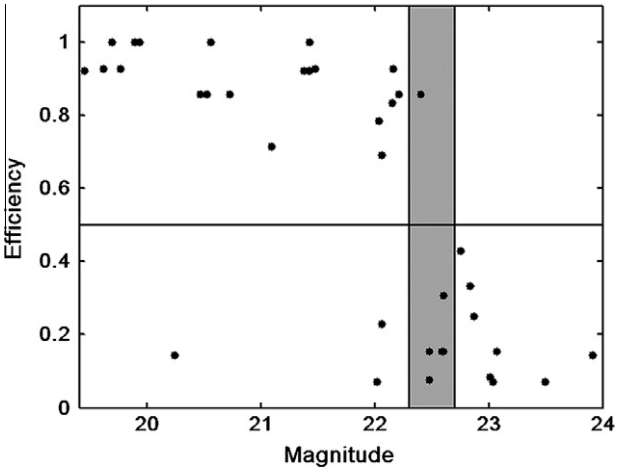

Fig. 5. The detection efficiency is the fraction of the 28 observers who detected implanted satellites of the magnitude on the x-axis. A reasonable upper limit is the magnitudes (shaded gray region) at which ~50% of the implanted satellites were found which is ~22.5 ± 0.4 magnitudes.

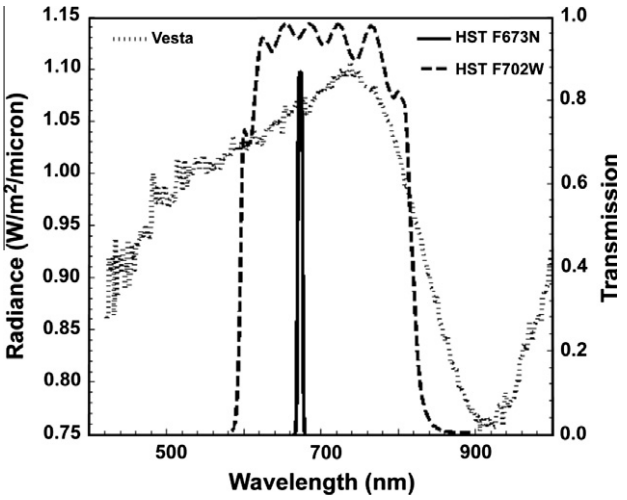

Fig. 6. The radiance of Vesta and the transmission curves of the 673N and 702W filters. The wide band pass of the 702W filter explains the high brightness of Vesta, 2.09 magnitudes, and the consequent small value of the upper limit on the radius of 22 ± 4 m.

poor by 23.5 magnitude. We chose 22.5 ± 0.4 as a reasonable single value for the upper limit of magnitude taking into account the range and sensitivities of all cameras.

5.3. Magnitude to radius calculations

The magnitude of an asteroid is related to its radius according to the relationship derived by Russell (1916). We calculated the radius associated with the above limiting magnitude assuming the albedo and phase function of Vesta are the same as the potential satellite. Then the ratio of the flux of the upper limit of the satellite to that of Vesta is simply the ratio of the squares of the radii. Expressing this in terms of magnitudes, we find:

$$r_{sat} = r_{Vesta}\sqrt{10^{-0.4(m_{sat}-m_{Vesta})}} \quad (3)$$

where r_{sat} and r_{Vesta} are the radii and m_{sat} and m_{Vesta} are the magnitudes for the satellite and Vesta respectively. Unfortunately, we did not measure the magnitude of Vesta through the F702W filter as we intentionally saturated Vesta to extend the search limit to large magnitude. However we converted the measured F673N magnitude of Vesta, $m(673N) = 5.96 \pm 0.01$, to that of the F702W filter, $m(702W) = 2.09 \pm 0.02$, by convolving the flux of Vesta at high spatial resolution from Xu et al. (1995) across the band passes of the two filters. The flux ratio of the two filter band passes is 35 ± 1 which we calculated from the reflectance spectrum of Vesta convolved with the solar spectrum and integrated over the band pass of the two filters. Our calculation was compared with filter calibration constants of WFPC2 cameras derived from the filter and system response multiplied by the solar spectrum (Karkoschka, 1998) and found to agree to ~14% confirming the magnitude of Vesta measured through the F702W filter derived here. The resulting high brightness of Vesta is realistic considering the width of the F702W filter (Fig. 6).

With a mean detection magnitude of 22.5 ± 0.4, the result is a satellite radius of 22 ± 4 m. The range in these values accounts for the range in magnitude detection limits found by the 28 observers on all of the WFPC2's cameras (Fig. 5).

6. Discussion

There are two points for discussion. First we consider the regions of previous searches compared to that reported here. The second point considers the absence of satellites compared to other observed asteroids with natural satellites.

We found Gradie and Flynn's (1988) search region was between 6000 and 100,000 km compared to the regions searched in this paper of 3710–68,900 km. We arrive at this statement by invoking an error in the units label of Gradie and Flynn's (1988), Table 1, that should read radius of the primary target, not units of kilometers (Gradie and Flynn, 1988). To justify this correction, we assumed units of asteroid primary radius for all entries in the table and calculated the minimum ranges in kilometers for all 17 asteroids observed with the same instrument, finding the minimum range to have been from ~5000 km to ~10,000 km, and the maximum ranges are from ~40,000 km to ~200,000 km. Since they used a single instrument to observe all asteroids, the range of search is determined by the field of view of the instrument and the region blocked by the coronagraph. For different asteroids, the conversion from instrument FOV to km depends on the observing range, and the variation is consistent with that range. The region searched by Gradie and Flynn does not reach closer to Vesta than the work reported here. Roberts et al. (1995) report they searched the region between 0.13 and 16.2 Vesta radii (35 and 4180 km). However, the inner region is the theoretical angular resolution of the telescope and neither this value nor the value r(max) includes instrumental effects. We plot their reported value and note that their reported size limit is 51 ± 2 km radius, four orders of magnitude larger than our search limit. None of the search regions adequately cover the region where the Dawn mission's spacecraft will be orbiting. It is important to search for satellites closer to Vesta than our observations allowed and deeper than the observations of both Roberts et al. (1995) and Gradie and Flynn (1988) for both scientific and mission safety reasons. There is justification to develop new methods of detecting satellites close to Vesta, for example, using the Keck Telescope with a coronograph (Li et al., 2010b) and the Dawn spacecraft.

The shape of Vesta shows a large basin in its southern hemisphere, suggesting that the asteroid experienced a significant impact in its past (Thomas et al., 1997a). The presence of vestoids, a group of asteroids ranging from 6 to 50 km in radius, which appear to have originated from Vesta because of their similar spectral properties (Binzel and Xu, 1993) and the existence of HED meteorites on Earth with evidence of multiple collisional ages (Eugster and Michel, 1995) possibly originating from Vesta, provide further evidence of debris-forming impacts. All of the above beg the question, "Why does Vesta *not* have satellites?" It is possible that a satellite formed during the same collision or collisions that produced the vestoids (Weidenschilling et al., 1989). However, none have been found to date. A satellite that may have remained in orbit around Vesta after an energetic collision event, may not be in an orbit that is stable over the time since the collision. Dynamical modeling of the formation and evolution of the Vesta family has focused on collisional velocities that result in fragments exceeding Vesta's escape velocity and subsequent pathways to Earth, not retaining bodies in orbit around Vesta. The (3) Juno and (4) Vesta families are believed to have formed by collision (Nesvorný et al., 2006), but there is no evidence of satellites having resulted from the family forming events. Tricarico and Sykes (2010) use different gravity models of Vesta to simulate the motion of the Dawn mission spacecraft around Vesta on a scale of 100 days. This study probes the lifetime of a satellite around Vesta, but the time interval is orders of magnitude smaller than is relevant to the stability of a natural satellite's orbit. The Pluto–Charon system is thought to have formed from an impact event, although velocities in the Kuiper belt are lower than that of the Main Asteroid belt (Weaver et al., 2006). No modeling has been carried out exploring the lifetime of natural satellites at Vesta on scales of significance for the history of the early Solar System. Life times on the order of billions of years need to be modeled to address the significance of the absence of satellites of Vesta.

Our search is defined by two characteristics: satellite size and the region searched. The lower radius limit of satellite size is 22 ± 4 m, a significant size limit when considered in comparison to the radius ratio of satellites found around other asteroids. Of the known asteroid binaries, the smallest radius ratio is 0.04 (Walsh, 2009). For Vesta, this corresponds to a radius of 10.5 km, yet our search is to a limit that is of order 1000 times smaller. Also, according to Weidenschilling et al. (1989), a satellite formed from a large impact would have formed close to the primary and would have a small mass ratio $\leqslant$0.01. Our search goes well below both of these limits assuming a satellite with the same properties as Vesta. Our search has been thorough within the region where satellites are likely to be gravitationally bound to Vesta.

Merline et al. (2002) note too that satellites of asteroids are most likely to be found close to the primary, with one known exception. The overwhelming majority of known asteroid – satellite pairs have a separation within 60 radii from the primary asteroid. Our search between 14 and 260 Vesta radii (3710 and 68,900 km) overlaps the region where satellites of other asteroids have been found in the past. The discovery of a satellite of Asteroid (41) Daphne at a distance of 5.5 asteroid radii (Merline et al., 2008) suggests that others probably exist close to the primary asteroid and have not been detected. We were unable to completely search the closest regions to Vesta because of detector saturation inside of 14 Vesta radii. The Dawn spacecraft orbits Vesta at multiple altitudes ranging from 2700 km (slightly more than 11 Vesta radii) down to <180 km ($\sim$1.6 Vesta radii). Satellite searches probing closer to Vesta's surface are warranted.

7. Conclusion

This search allowed us to set limits on the size and magnitude of natural satellites in orbit around Asteroid (4) Vesta in the region searchable with Hubble Space Telescope's WFPC2 in May 2007. The detection limits vary from camera to camera, but our 28 volunteer testers searching for implanted, synthetic satellites found almost all of the objects brighter than 22.5 ± 0.4. Vesta's albedo at 700 nm is 0.47 and assuming the satellite's albedo is the same as that of Vesta at the same wavelength, this limit corresponds to a photometric radius of 22 ± 4 m. The outer edge of the region searched is about half of the Hill sphere and most of the region where satellites are expected to be gravitationally bound. The region within 14 Vesta radii was not explored however, due to saturation of Vesta. This search is important for NASA's Dawn mission because it will spend months in close proximity to Vesta (Fig. 1). The region searched prior to the Dawn mission, does not extend close enough to Vesta to eliminate possible threats to the Dawn spacecraft (Rayman et al., 2006). A dedicated satellite search of Vesta by Dawn's imaging camera is warranted for both scientific interest and mission operations.

Acknowledgments

Support for this work was provided by NASA through GO 10799 from the Space Telescope Science Institute, which is operated by the Association of Universities for Research in Astronomy, Inc., under NASA Contract NAS5-26555.

We thank our program coordinator, William Januszewski and staff at Space Telescope Science Institute for making these observations possible. L.A.M. acknowledges partial support for this work by the Dawn Project under contract from UCLA to University of Maryland 2090SJB692. Reviews by Susan Benecchi and Bill Merline were very helpful.

References

Asphaug, E., 1997. Impact origin of the Vesta family. Meteorit. Planet. Sci. 32, 965–980.
Binzel, R.P., Xu, S., 1993. Chips off of Asteroid 4 Vesta: Evidence for the parent body of basaltic achondrite meteorites. Science 260, 186–191.
Cox, A.N., 2000. Allen's Astrophysical Quantities, fourth ed. Springer-Verlag, New York.
Durda, D.D., Bottke Jr., W.F., Enke, B.L., Merline, W.J., Asphaug, E., Richardson, D.C., Leinhardt, Z.M., 2004. The formation of asteroid satellites in large impacts: Results from numerical simulations. Icarus 167, 382–396.
Eugster, O., Michel, Th., 1995. Common asteroid break-up events of eucrites, diogenites and howardites and cosmic-ray production rates for noble gases in achondrites. Geochem. Cosmochim. Acta 59, 177–199.
Feierberg, M.A., Drake, M.J., 1980. The meteorite–asteroid connection: The infrared spectra of eucrites, shergottites, and Vesta. Science 209, 805–807.
Gehrels, T., Drummond, J.D., Levenson, N.A., 1987. The absence of satellites of asteroids. Icarus 70, 257–263.
Gonzaga, S., Biretta, J., et al., 2010. HST WFPC2 Data Handbook, V. 5.0. STScI, Baltimore.
Gradie, J., Flynn, L., 1988. A search for satellites and dust belts around asteroids: Negative results. Lunar Planet. Sci. XIX. Abstract 405.
Hamilton, D.P., Burns, J.A., 1991. Orbital stability zones about asteroids. Icarus 92, 118–131.
Joye, W.A., Mandel, E., 2003. New features of SAOImage DS9. In: Payne, H.E., Jedrzejewski, R.I., Hook, R.N. (Eds.), Astronomical Data Analysis Software and Systems XII ASP Conference Series, vol. 295, p. 489.
Karkoschka, E., 1998. WFPC2 Photometry for the Solar System. <http://www.stsci.edu/hst/wfpc2/analysis/wfpc2_ss_phot.html>.
Li, J.-Y., McFadden, L.A., Thomas, P.C., Mutchler, M.J., Parker, J.W., Young, E.F., Russell, C.T., Sykes, M.V., Schmidt, B.E., 2010a. Photometric mapping of Asteroid (4) Vesta's southern hemisphere with Hubble Space Telescope. Icarus 208, 238–251.
Li, J.-Y., Crepp, J., Serabyn, G., McFadden, L., Williams, J., Crow, C., 2010b. Search for satellites around asteroids with coronagraphic high-contrast imaging on adaptive optics. Bull. Am. Astron. Soc. 42, 1038 (American Astronomical Society, DPS Meeting #42, #39.30).
Li, J.-Y., Bodewits, D., Feaga, L.M., Landsman, W., A'Hearn, M.F., Mutchler, M.J., Russell, C.T., McFadden, L.A., Raymond, C.A., 2011. UV spectroscopy of Asteroid (4) Vesta. Icarus 216, 640–649.
McCord, T.B., Adams, J.B., Johnson, T.V., 1970. Asteroid Vesta: Spectral reflectivity and compositional implications. Science 168, 1445–1447.
McMaster, M., Biretta, J., et al., 2008. WFPC2 Instrument Handbook, Version 10.0. STSCI, Baltimore.
Merline, W.J., Weidenschilling, S.J., Durda, D.D., Margot, J.L., Pravec, P., Storrs, A.D., 2002. Asteroids do have satellites. In: Bottke, W.F., Cellino, A., Paolicchi, P., Binzel, R.P. (Eds.), Asteroids III. The University of Arizona Press, Tucson, pp. 289–312.
Merline, W.J. et al., 2008. Discovery of an extreme mass-ratio satellite of (41) Daphne in a close orbit. ACM Meeting, Baltimore, 2008, LPI Contribution No. 1405. Paper Id. 8370.
Nesvorný, D., Bottke, W.F., Vokrouhlický, D., Morbidelli, A., Jedicke, R., 2006. Asteroid families. In: Lazzaro, D., Ferraz-Mello, S., Fernandez, J.A. (Eds.), Asteroids, Comets, Meteors. Proc. IAU Symposium No. 229, 2005, pp. 289–299.
Rayman, M.D., Fraschetti, T.C., Raymond, C.A., Russell, C.T., 2006. Dawn: A mission in development for exploration of main belt Asteroids Vesta and Ceres. Acta Astronaut. 58, 605–616.
Roberts, L.C., McAlister, H.A., Hartkoff, W.I., 1995. Speckle interferometric survey for asteroid duplicity. Astron. J. 110, 2463–2468.
Russell, H.N., 1916. On the albedo of planets and their satellites. Astrophys. J. 43, 173–196.
Shevchenko, V.G., Tedesco, E.F., 2006. Asteroid albedos deduced from stellar occultations. Icarus 184, 211–220.
Steffl, A.J. et al., 2006. New constraints on additional satellites of the Pluto system. Astron. J. 132, 614–619.
Tedesco, E.F., Noah, P.V., Noah, M., Price, S.D., 2002. The supplemental IRAS minor planet survey. Astron. J. 123, 1056–1085.
Thomas, P.C., Binzel, R.P., Gaffey, M.J., Storrs, A.D., Wells, E.N., Zellner, B.H., 1997a. Impact excavation on Asteroid 4 Vesta: Hubble Space Telescope results. Science 277, 1492–1495.
Thomas, P.C., Binzel, R.P., Gaffey, M.J., Zellner, B.H., 1997b. Vesta: Spin pole, size and shape from HST images. Icarus 128, 88–94.
Tricarico, P., Sykes, M.V., 2010. The dynamical environment of Dawn at Vesta. Planet. Space Sci. 58, 1516–1525.
Walsh, K.J., 2009. Asteroids with satellites: Inventory, properties, and prospects for future discoveries. Earth Moon Planets 105, 193–199.
Weaver, H.A. et al., 2006. The discovery of two new satellites of Pluto. Nature 439, 943–945.
Weidenschilling, S.J., Paolicchi, P., Zappalà, V., 1989. Do asteroids have satellites? In: Binzel, R.P., Gehrels, T., Matthews, M.S. (Eds.), Asteroids II. The University of Arizona Press, Tucson, pp. 643–658.
Xu, S., Binzel, R.P., Burbine, T.H., Bus, S.J., 1995. Small main-belt asteroid spectroscopic survey: Initial results. Icarus 115, 1–35.